Deuterium NMR relaxation in the smectic-*A* phase of a chiral smectogen

Ronald Y. Dong,[1,*] L. Chiezzi,[2] and C. A. Veracini[2]
[1]*Department of Physics and Astronomy, Brandon University, Brandon, Manitoba, Canada R7A 6A9*
[2]*Dipartimento di Chimica e Chimica Industriale, Universita degli Studi di Pisa, via Risorgimento 35, 56126 Pisa, Italy*
(Received 10 September 2001; published 10 April 2002)

Correlated internal rotations are studied for a deuterated decyloxy chain in the chiral liquid crystal, 1-methylheptyl 4′-(4-*n*-decyloxy-benzoyloxy)biphenyl-4-carboxyate (10B1M7) using deuteron spin-lattice relaxation and quadrupolar splitting measurements. The present study is limited to the uniaxial smectic-*A* phase of 10B1M7, in which the observed deuterium nuclear magnetic resonance spectra show well-resolved peaks. The deuteron Zeeman (T_{1Z}) and quadrupolar (T_{1Q}) spin-lattice relaxation times are simultaneously determined for the methylene deuterons using the Wimperis broadband pulse sequence at two different Larmor frequencies. The quadrupolar splittings at each temperature are modeled by the additive potential method to obtain the orienting potential of mean torque. A decoupled model using 683 conformations for the decyloxy chain is used to explain the observed relaxation rates. In this model, the overall reorientation is described by a small step rotational diffusion model, while both *gauche* migration and *gauche* pair production as well as the so called one- and two-bond motions are allowed to occur in the chain. Transition rates for the chain dynamics and the overall rotational diffusion constants are obtained using a global target analysis of the relaxation data of 10B1M7.

DOI: 10.1103/PhysRevE.65.041716 PACS number(s): 61.30.−v

I. INTRODUCTION

Chiral liquid crystals can give rise to ferroelectric (FLC) and antiferroelectric (AFLC) phases as well as some interesting new chiral subphrases. These materials have recently attracted much attention [1–8] because of their possible technological applications and some interesting microscopic structures found in these newer materials. Many experimental methods have been employed to study the molecular behaviors of FLC and AFLC and phases inbetween. Among these, nuclear magnetic resonance (NMR) spectroscopy [9] is by far more superior in elucidating molecular ordering and dynamics in flexible liquid crystals. Both carbon-13 [10,11] and deuteron [12–15] NMR have been employed to study chiral liquid crystals. In the present study, we have chosen to study a particular isotopomer of an optically pure chiral smectogen 1-methylheptyl 4-(4-*n*-decyloxy-benzoyloxy)biphenyl-4-carboxyate (10B1M7) in which the achiral decyloxy chain has been perdeuterated.. The chiral heptyl chain of 10B1M7 molecule has not been deuterated. The deuterium NMR spectra of aligned liquid crystals usually show well-resolved doublets. However, upon decreasing the temperature of 10B1M7 into its AFLC the linewidths drastically increase to such an extent that doublets from the deuterons near the beginning of the chain become seriously overlapped. Thus, the present study is limited to its smectic-*A* (Sm *A*) phase. Now the partially relaxed deuterium spectra are dominated by the intramolecular quadrupolar interactions of isolated spin-1 nuclei. As in liquids, mesogenic molecules can translationally diffuse, reorient as a whole, and have internal conformational changes. However, motional anisotropies can now exist inside liquid crystalline phases because of the anisotropic intermolecular potential. Although collective fluctuations known as order director fluctuations (ODF) [16,17] can relax nuclear spins in liquid crystals, they are usually important in non-viscous nematic phases. Furthermore, being collective hydrodynamical deformations involving many molecules ODF represent very slow dynamics and are most effective in the low frequency (kHz) regime. Hence, in the Sm-*A* phase of 10B1M7 at 15.1 and 46 MHz, ODF will be neglected as a possible relaxation mechanism. Also relaxation due to translational self-diffusion is of intermolecular nature, and therefore does not affect deuteron spins. As a consequence, only molecular reorientations of the whole molecule and correlated internal rotations in the deuterated decyloxy chain are needed to understand relaxation behaviors of deuterons in 10B1M7-d_{21}. The reorientation of molecules in liquid crystals can be described by the rotational diffusion model [18–20]. Here we adopt the Nordio model, but with the extension to a biaxial probe [21]. Each molecule is characterized by a rotational diffusion tensor whose principal elements are defined in a frame fixed on the molecule. The internal bond rotation motions within the side chain must be considered in order to fully understand nuclear spin relaxation in liquid crystals. To this end, a decoupled model, which described correlated internal bond rotations and the overall reorientation of molecules being independent of each other, was proposed independently by us [22] and Nordio and co-workers [23] about a decade ago for 4-*n*-pentyl-4′-cyanobiphenyl (5CB).

In our model, a master equation was used to describe transitions among various chain conformations, which must first be generated using the rotameric state (RIS) model of Flory [24]. The rotational diffusion tensor was assumed to be the one for an ''average'' conformer. In other words, the diffusion tensors for different conformers do not deviate substantially from each other. Allowable transitions are generated by three different types of bond motions, viz. one-bond (k_1), two-bond (k_2), and three-bond (k_3) motions [22]. We

*Email address: dong@brandonu.ca

further assume that one phenomenological rate constant is sufficient to describe each type of bond motion. The decoupled model has successfully been used to understand the internal dynamics of flexible chain(s) in many different liquid crystals studied by the proton [25] and deuteron [26–35] spin relaxation. The liquid crystals used to critically test the decoupled model include calamitics, discotics and metallomesogens of different chain lengths. These studies have shown that the three-bond motion tends to give rather high k_3 (about 10^{17}–10^{18} s^{-1}) values in some of the studied materials. To overcome the apparent high k_3 rate, a modified decoupled model was recently proposed [36,37] in which the three-bond motion is replaced by the type-II motion of Helfand [38]. Helfand has classified conformational transitions in the chain into three different types (type-I, -II and -III motions). His type-III motion consists of two kinds, i.e., one-bond (k_1) motion given by $\{ijklm\}\rightarrow\{ijklm'\}$, and the two-bond ($k_2$) motion by $\{ijklm\}\rightarrow\{ijkl'm'\}$, where $\{ijklm\}$ denotes a configuration of the carbon-carbon backbone of a pentyl chain. The type-II motion also consists of two kinds, viz $ttt\rightarrow g^{\pm}tg^{\mp}$ is a *gauche* pair production or a kink formation, and $ttg\rightarrow gtt$ is a *gauche* migration. This particular motion does not swing the chain but the chain does translate. The type-I (or the three-bond rotation and crankshaft motion) motion should call for high activation energies [39,40] because several bonds must be activated almost simultaneously. Thus the type-I motion was totally discarded in the modified decoupled model. The modified decoupled model also uses a reduced number of configurations by considering only those configurations that are significantly populated in anticipation of applying the model to a long side chain. This has been successfully applied to two members of 4-*n*-alkyloxy-4′-cyanobiphenyl (*n*OCBZ,$n=6$ and 8) [37]. One of the aims of this study is to check the model for a decyloxy chain, at least in the high temperature Sm-*A* phase of 10B1M7. The paper is organized as follows. Section II gives a brief description of the modified decoupled model and the additive potential (AP) method for modeling the quadrupolar splittings. Section III outlines the experimental method. Section IV gives the results and discussion.

II. THEORY

The complete description of the formulas necessary to discuss the deuteron quadrupolar splitting and spectral density data can be found in the literature [9,22]. The molecular mean field theory based on the AP method [41], the small-step rotational diffusion model for biaxial probes [21] and the decoupled model [22,36] are used in this study. Only formulas needed to explain our experimental data will be outlined here. For an alkyloxy chain, the O—C_α bond is taken to be fixed on the phenyl ring plane with a C_{ar}–O–C_α angle of 126.4° where the subscript *ar* denotes aromatic, and the ∠C–C–C, ∠C–C–H, and ∠H–C–H are assumed to be 113.5°, 107.5°, and 113.6°, respectively [42]. The O—C bond is treated same as a C—C bond, and the ∠O–C–C is set the same as ∠C–C–C. The dihedral angles $\phi=0$, $\pm 112°$ are for rotation about each C—C bond and also about the O—C bond in the alkyloxy chain. The geometry of the molecule is needed in the AP method [42] to construct the external mean potential $U_{ext}(n,\Omega)$ for the conformer *n* at the orientation Ω with respect to the nematic director. In addition, the interaction tensors for the molecular core (which consists of the aromatic fragments including the chiral chain) and for each C—C bond are assumed to be cylindrically symmetric, and characterized by the parameters X_a and X_{cc}, respectively. The C_{ar}—O bond is included with the molecular core when calculating its interaction energy. Among possible conformations generated using Flory's RIS, a lot of them are energetically unfavorable. In an effort to limit conformations to those with relatively high probabilities, a decyloxy chain, which contains six or more *gauche* C—C bonds, can be safely ignored. Even the conformations with two consecutive *gauche* C—C bonds (i.e., $g^{\pm}g^{\pm}$ and $g^{\pm}g^{\mp}$) can be ignored. With these assumptions, the number of conformations (*N*) in 10B1M7 is 683. This represents a great reduction from the possible maximum number of 19 683. In principle, those less favorable conformations can be included if desired.

The segmental order parameter of the C—D bond ($S_{\mathrm{CD}}^{(i)}$) at *i*th carbon site is calculated from the quadrupolar splitting $\Delta\nu_i$ according to the relation

$$\Delta\nu_i=\tfrac{3}{2}q_{\mathrm{CD}}^{(i)}S_{\mathrm{CD}}^{(i)}, \tag{1}$$

where $q_{\mathrm{CD}}=e^2qQ/h$ is the quadrupolar coupling constant. For the methylene deuterons, $q_{\mathrm{CD}}^{(i)}=165$ kHz is taken and the asymmetry parameter η of the electric-field-gradient tensor is zero. To model the quadrupolar splittings along the flexible chain, the potential of mean torque $U(n,\Omega)$ is written as

$$U(n,\Omega)=U_{int}(n)+U_{ext}(n,\Omega), \tag{2}$$

where the internal energy $U_{int}(n)$ is given by the number of *gauche* linkages and E_{tg}, the energy difference between a *gauche* state and a *trans* state in the chain. Note that the E_{tg}(OCC) is higher than the E_{tg}(CCC) due to the presence of the oxygen in the chain. Now the segmental order parameter $S_{\mathrm{CD}}^{(i)}$ is a weighted average of the segmental order parameter $S_{bb}^{n,i}$ for the C_i—D bond ($i=1$ is for the carbon near the ring) of the molecule having the conformer *n*

$$S_{CD}^{(i)}=\sum_{n=1}^{N}P_{eq}(n)S_{bb}^{n,i}, \tag{3}$$

where the *b* axis of the principal axis frame (a,b,c) of the nuclear quadrupolar interaction is taken to be along the methylene C—D bond, and $P_{eq}(n)$ is the equilibrium probability of the conformer *n*. By modeling the segmental order profile using Eq. (3) at each temperature, the interaction parameters X_a and X_{cc} used in $U_{ext}(n,\Omega)$ can be determined. Simultaneously the order parameter tensor for an "average" conformer of the molecule can also be evaluated [9].

It is generally accepted that a second-rank pseudopotential $U(\Omega)$ can be used to solve the rotational diffusion problem of a rigid rodlike molecule. For uniaxial phases, the orientating potential for a biaxial probe is independent of the

Euler angle α and $U(\Omega)$ can be parameterized by two second-rank coefficients a_{20} and a_{22} [21]

$$\frac{U(\beta,\gamma)}{k_BT}=a_{20}\left(\frac{3}{2}\cos^2\beta-\frac{1}{2}\right)+a_{22}\sqrt{\frac{3}{2}}\sin^2\beta\cos 2\gamma, \tag{4}$$

where $a_{2-2}=a_{22}$ is used. The molecular biaxial parameter $\xi=a_{22}/a_{20}$ is a measure of the deviation from cylindrical symmetry for the biaxial molecule. When a_{22} is set to zero as in the Nordio model, the orienting potential is identical to the Maier-Saupe potential. In principle, the coefficients a_{20} and a_{22} can be determined from a knowledge of order parameters $S_{zz}(\langle P_2\rangle)$ and $S_{xx}-S_{yy}$. For flexible molecules, the orienting potential is first established from the order tensor of an ''average'' conformer. The $P_{eq}(n)$ obtained from fitting the chain splittings is used to weigh transitions between different conformational states when treating spin relaxation of chain deuterons. In setting up the transition rate matrix $\overline{\overline{R}}$ among the N conformations, the following conditions are imposed [36] as before. (1) No direct transition between g^+ and g^- states as this costs too much energy; (2) transitions between $gtgtt$ and $tgtgt$ cannot proceed directly as these also cost too much energy (however, $gtgtt \rightleftharpoons ttttt \rightleftharpoons tgtgt$ are possible); and (3) no three-bond (k_3) motion is allowed. There are 2776 transitional elements in $\overline{\overline{R}}$ when considering both forward and reverse transitions. Among the 1388 forward transitions, there are 342 type-III motions about the C_8—C_9 bond (k_1 motions), 170 type-III motions about the C_7—C_8 bond (k_2 motions), and 876 type-II motions. For the latter type, 438 transitions are for the *gauche* migration (e.g., $ttttg^{\pm}tt \rightleftharpoons ttg^{\pm}tttt$) and 438 transitions are for the kink formation (e.g., $ttttttt \rightleftharpoons ttg^-tg^+tt$). Again we assume a single rate constant k_g for a *gauche* migration, and k_g' for formation or removing a kink in the chain. In comparison with the original decoupled model, we have inevitably introduced an extra rate constant for the internal dynamics. It is noted that the modified decoupled model differs from the old one only in the way one constructs the transition rate matrix, and formal expressions for the spectral densities remain, therefore, unchanged. Thus the spectral densities for the C_i deuterons on the chain can be written for $m>0$ as

$$\begin{aligned}J_m^{(i)}(m\omega)=&\frac{3\pi^2}{2}(q_{CD}^{(i)})^2\sum_n\sum_{n'}\sum_{k=1}^{N}\left(\sum_{l=1}^{N}\sum_p d_{n0}^2(\theta_{N,Q}^{(i)l})d_{np}^2(\theta)\exp[-in\psi_{N,Q}^{(i)l}]x_l^{(1)}x_l^{(k)}\right)\\&\times\left(\sum_{l'=1}^{N}\sum_{p'} d_{n',0}^2(\theta_{N,Q}^{(i)l'})d_{n'p'}^2(\theta)\exp[-in'\psi_{N,Q}^{(i)l'}]x_{l'}^{(1)}x_{l'}^{(k)}\right)\\&\times\sum_j\frac{(\beta_{mnn'}^2)_j[(\alpha_{mnn'}^2)_j+|\lambda_k|]}{m^2w^2+[(\alpha_{mnn'}^2)_j+|\lambda_k|]^2},\end{aligned} \tag{5}$$

where $\theta_{N,Q}^{(i)l}$ and $\psi_{N,Q}^{(i)l}$ are the polar angles for the C_i—D bond of the conformer l in the molecular N frame fixed on the phenyl ring core, θ is the angle between the Z_N axis (along the para axis of the phenyl ring) and the long molecular axis (Z_M) of 10B1M7, λ_k and $\vec{x}^{(k)}$ are the eigenvalues and eigenvectors from diagonalizing $\overline{\overline{R}}$, and $(\alpha_{mnn'}^2)_j/D_\perp$, the decay constants, and $(\beta_{mnn'}^2)_j$, the relative weights of the exponentials in the correlation functions, are the eigenvalues and eigenvectors from diagonalizing the matrix of the rotational diffusion operator [21]. The rotation diffusion constants $D_\parallel$ and $D_\perp$ are for rotation of the molecule about its long axis, and for rotation about one of its short axes, respectively, and they appear in Eq. (5) through the decay constants $(\alpha_{mnn'}^2)_j$.

III. EXPERIMENTAL METHOD

The synthesis of 10B1M7 was performed following the generic route given by Goodby *et al.* [4] and Ref. [13]. The transition temperatures reported [4] in °C are 124.5, 105.4, 75.9, 69, and 47.8 for isotropic–Sm-*A*, Sm-*A*–Sm-C*, Sm-C*–Sm *J**, Sm-*J**–AFLC, and AFLC-ferrielectric transitions repectively. The corresponding transition temperatures for our isotopomer 10B1M7-d_{21} (see Fig. 1) are slightly lower.

A home-built superheterodyne coherent pulse NMR spectrometer was operated for deuterons at 15.1 MHz using a Varian 15-in electromagnet and at 46.05 MHz using a 7.1-T Oxford superconducting magnet. The temperature gradient across the sample in the NMR probe was estimated to be better than 0.3 °C. The $\pi/2$ pulse width is about 4 μs. Pulse control and signal collection were performed by a GE 1280 minicomputer. Broadband Wimperis sequence [43] was used to simultaneously measure the T_{1Z} and T_{1Q} spin-lattice relaxation times. The pulse sequence was modified using an additional monitoring $\pi/4$ pulse to minimize any long-term instability of the spectrometer. Signal collection was started 10 μs after each monitoring $\pi/4$ pulse, and averaged over 48 to 320 scans at 46 MHz and up to 4800 scans at 15.1 MHz depending on the signal strengths. The description of data reductions has been previously described [44]. The experimental accuracy in measuring the relaxation times is estimated to be about 5%. Quadrupolar splittings were mea-

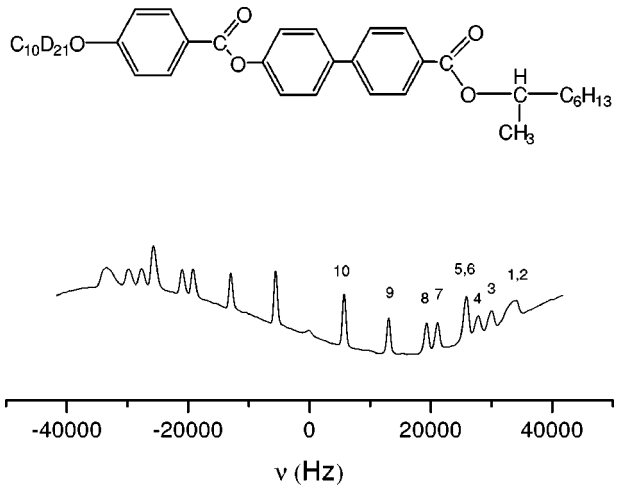

FIG. 1. A typical deuteron NMR spectrum of 10B1M7-d_{21} and its schematic structure. The spectrum collected in the smectic-*A* phase also shows the tentative peak assignment.

sured from spectra by fast Fourier transformation of free induction decays obtained by a single $\pi/2$ pulse.

IV. RESULTS AND DISCUSSION

Figure 1 shows a typical deuteron NMR spectrum obtained in the Sm-*A* phase of 10B1M7-d_{21} sample. The peak assignments are based on the assumption that the splittings decrease monotonically down the chain. It should be pointed out that the deuteron signals from C_1 and C_2 are broad and overlapped so that their individual quadrupolar splittings (and their spectal densities) cannot be measured separately, and a single splitting is estimated for both sites with a relatively high uncertainty. Also the deuteron signals from C_5 and C_6 occur on top of each other. Figure 2 shows the experimental segmental order parameter $S_{\mathrm{CD}}^{(i)}$ versus the temperature for the achiral chain. An optimization routine (AMOEBA) [45] was used to minimize the sum squared error f in fitting the segmental order parameters (or quadrupolar splittings)

$$f=\sum_i \left(|S_{\mathrm{CD}}^{(i)}|-|S_{\mathrm{CD}}^{(i)calc}|\right)^2, \tag{6}$$

where the sum over i includes C_1 to C_9. The E_{tg} values for C-C-C-C and C-O-C-C are set at 3800 J/mole and 5700 J/mol, which are comparable to values used in other liquid crystals [37]. The f values at different temperatures are of the order of 10^{-3} (see Table I).The calculated segmental order parameters are indicated in the figure as solid and dashed lines. It is obvious that some systematic deviations exist in the fitting process, but our aim is not to produce a perfect fit of the quadrupolar splittings. A possible explanation of these deviations may be due to the small number of configurations and the assumptions inherent in the AP method. We tabulate X_a, X_{cc}, f, and the order parameters $\langle P_2\rangle$ and $\langle S_{xx}-S_{yy}\rangle$ for the ''average'' conformer of 10B1M7 in Table I, and find that these model parameters are sufficient for treating the relaxation data. Our $\langle P_2\rangle$ values compare favorably with

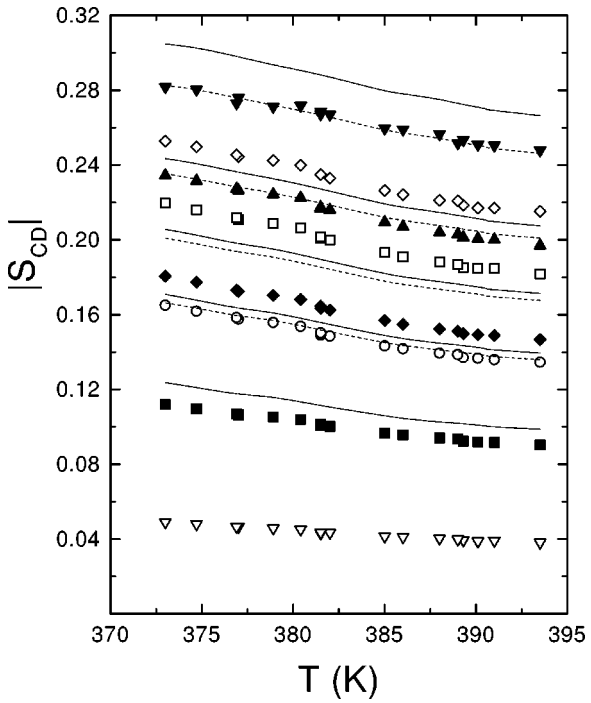

FIG. 2. Plot of segmental order parameters of 10B1M7-d_{21} versus the temperature. Solid down-triangles, up-triangles, diamonds, and squares denote $C_{1,2}$, C_4, C_7, and C_9 sites, respectively. Open diamonds, squares, circles, and down-triangles denote C_3, $C_{5,6}$, C_8, and C_{10} sites, respectively. The dashed curves are the theoretical calculations for C_2, C_4, C_6, C_8 starting from the top, while solid curves are the theoretical calculations for C_1, C_3, C_5, C_7, and C_9 starting from the top.

those obtained in a previous study of 10B1M7 based on the spectral data from the phenyl ring which is attached directly to the decyloxy chain [13]. The angle between the para axes of phenyl and biphenyl fragments was also estimated in the same study to be about 15° in the Sm-*A* phase. The long molecular axis is taken to roughly bisect this angle. Thus, the θ angle that appears in Eq. (5) has been set to 8°.

The experimental spectral densities for 10B1M7-d_{21} versus the temperature are plotted in Fig. 3. We have carried out

TABLE I. Model parameters derived from the analysis of quadrupolar splittings in 10B1M7-d_{21}. The interaction parameters X_a and X_{cc} are in J/mol.

T(K)	X_a	X_{cc}	$\langle P_2\rangle$	$\langle S_{xx}-S_{yy}\rangle$	$10^3 f$
373.0	10 330	795.4	0.758	0.0152	3.1
374.7	10 374	779.1	0.757	0.0148	3.0
377.0	10 108	760.9	0.748	0.0152	3.0
378.9	9721	764.6	0.736	0.0164	3.2
381.5	9614	734.9	0.729	0.0161	2.7
385.0	9126	709.7	0.709	0.0171	2.7
388.0	9039	693.3	0.702	0.0171	2.5
390.1	8747	686.5	0.689	0.0179	2.4
391.0	8728	687.7	0.688	0.0180	2.7
393.5	8620	685.9	0.681	0.0184	2.6

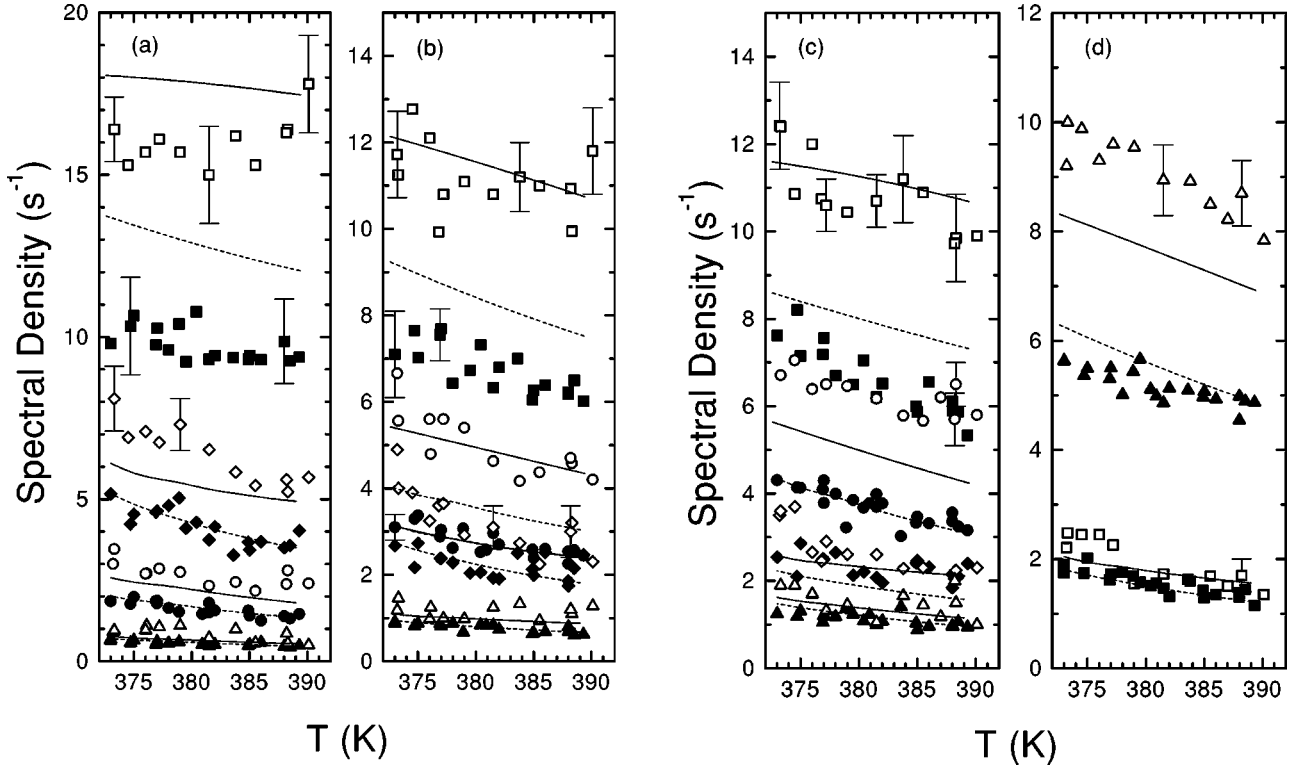

FIG. 3. Plots of spectral densities versus the temperature in 10B1M7-d_{21}. Open and closed symbols denote data collected at 15.1 MHz and 46 MHz, respectively. Solid and dashed curves are calculated spectral densities for 15.1 and 46 MHz, respectively. (a) Squares and diamonds denote $J_1(\omega)$ and $J_2(2\omega)$, respectively, measured for $C_{1,2}$, while circles and triangles denote $J_1(\omega)$ and $J_2(2\omega)$, respectively, measured for C_9. Solid (dashed) curves are for $J_1(\omega)$ and $J_2(2\omega)$ of $C_{1,2}$ and of C_9 starting from the top; (b) squares and diamonds denote $J_1(\omega)$ and $J_2(2\omega)$, respectively, measured for C_3, while circles and triangles denote $J_1(\omega)$ and $J_2(2\omega)$, respectively, measured for C_8. Solid (dashed)curves are for $J_1(\omega)$ and $J_2(2\omega)$ of C_3 and of C_8 starting from the top; (c) squares and diamonds denote $J_1(\omega)$ and $J_2(2\omega)$, respectively, measured for C_4, while circles and triangles denote $J_1(\omega)$ and $J_2(2\omega)$, respectively, measured for C_7. Solid (dashed) curves are for $J_1(\omega)$ and $J_2(2\omega)$ of C_4 and of C_7 starting from the top; (d) triangles and squares denote $J_1(\omega)$ and $J_2(2\omega)$, respectively, measured for $C_{5,6}$. Solid (dashed) curves are for $J_1(\omega)$ and $J_2(2\omega)$ of $C_{5,6}$. Some typical error bars are shown.

individual target analysis (fitting data at a single temperature) using Eq. (5) to get an idea of the temperature behaviors of various model parameters. As a result, we take in our initial global target analysis simple Arrhenius-type relations for all model parameters to give

$$D_\perp = D_\perp^0 \exp[-E_a^{D_\perp}/RT], \tag{7}$$

$$D_\parallel = D_\parallel^0 \exp[-E_a^{D_\parallel}/RT], \tag{8}$$

$$k_i = k_i^0 \exp[-E_a^{k_i}/RT], \tag{9}$$

$$k_g = k_g^0 \exp[-E_a^{k_g}/RT], \tag{10}$$

$$k_g' = k_g'^0 \exp[-E_a^{k_g'}/RT], \tag{11}$$

where $i=1$ or 2, $D_\perp^0$, $D_\parallel^0$, k_i^0, k_g^0 and $k_g'^0$ are the preexponential constants and E_a with an appropriate superscript is the corresponding activation energy. The preexponential constants and activation energies form the set of 12 target parameters to be derived from fitting the spectral densities of C_1 to C_9 deuterons at 15.1 and 46 MHz and nine temperatures covering the Sm-*A* phase. As correlation coefficients between preexponentials and their corresponding activation energies are close to 1, Eqs. (7)–(11) were rewritten in terms of the activation energies and the diffusion ($D_{\perp t}, D_{\parallel t}$) and jump constants ($k_{1t}, k_{2t}, k_{gt}, k'_{gt}$) at an arbitrary chosen temperature T_{ref} (389 K). These now formed the target parameters used in the global target analyses. In fitting the smoothed experimental spectral densities, we minimized the mean-squared percent deviation F with AMOEBA. The fitting quality factor Q is defined by

$$Q = \frac{\sum_k \sum_\omega \sum_i \sum_m [J_m^{(i)calc}(m\omega) - J_m^{(i)expt}(m\omega)]_k^2}{\sum_k \sum_\omega \sum_i \sum_m [J_m^{(i)expt}(m\omega)]_k^2}, \tag{12}$$

where the sum over k is for nine temperatures. We obtained a Q value of 2.8%. The rotational diffusion constants and jump rate constants are plotted in Fig. 4, while the calculated spectral densities for various sites are shown as solid and dashed curves in Fig. 3. The agreement between the calculated and experimental spectral densities is good for $J_1(\omega)$ and/or

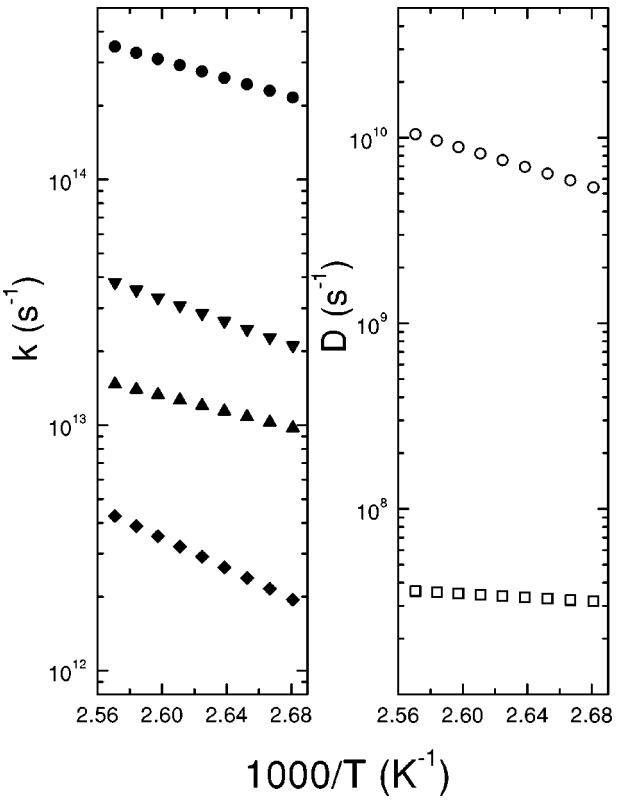

FIG. 4. Plots of jump rate constants k_1 (up-triangles), k_2 (circles), k_g (down-triangles) and k_g' (diamonds), as well as rotational diffusion constants $D_\parallel$ (circles) and $D_\perp$ (squares) as a function of the reciprocal temperature.

$J_2(2\omega)$ for some sites, but some systematic deviations do exist for other sites. We believe that these discrepancies may be due to the many simplifying assumptions in our models. For instance, the number of conformations could be increased, which may help to improve the Q value. The goodness of the present fits may be justified by comparing the derived jump rates and rotational diffusion constants for this smectogen with those in the literature [37]. The apparent activation energies $E_a^{D_\perp}$, $E_a^{D_\parallel}$, $E_a^{k_1}$, $E_a^{k_2}$, $E_a^{k_g}$, and $E_a^{k_g'}$ are 9.5, 49.6, 31.1, 35.9, 44.6, and 59.1 kJ/mol, respectively. The rotational diffusion constants were reported [15] based on the ring data from two different ring deuterated isotopomers of 10B1M7. Some uncertainties were noted for both $D_\perp$ and $D_\parallel$ in this study. The $D_\perp$ values obtained here coincide closely to those of case (3) in Ref. [15], although our $D_\parallel$ values are about a factor of 3 larger. It would appear that larger number of spectral densities can facilitate more unique determination of the overall motion. As noted in Fig. 4, all jump rates are about or less than 10^{14} s^{-1}. It is not unreasonable to expect the internal bond rotations to be two or more orders of magnitudes faster than the spinning motion of a relatively large molecule like 10B1M7. The preexponentials in Eq. (7)–(11) are calculated as follows: $k_1^0=2.19\times10^{17}$ s^{-1}, $k_2^0=2.33\times10^{19}$ s^{-1}, $k_g^0=3.72\times10^{19}$ s^{-1}, $k_g'^0=3.70\times10^{20}$ s^{-1}, $D_\perp^0=6.83\times10^8$ s^{-1}, $D_\parallel^0=4.85\times10^{16}$ s^{-1}. We now address the error limits for our derived model parameters. The error limit for a particular global parameter was estimated by varying the one under consideration while keeping all other global parameters identical to those for the minimum F, to give an approximate doubling in the F value. Certain model parameters are relatively insensitive in the fits. These error limits given in parentheses are for an increase of 75% in the F value. In fact, we found that both the upper bound of k_2^0 and the lower bound of $E_a^{k_2}$ cannot be estimated, while the lower bound of k_2^0 is 9×10^{17} s^{-1} and the upper bound of $E_a^{k_2}$ is 46.3 kJ/mol. The error limits for k_1^0 lie between 5.5×10^{16} s^{-1} and (6.0×10^{18} s^{-1}) and the corresponding activation energy $E_a^{k_1}$ lies between (20.5 kJ/mol) and 35.5 kJ/mol. Now 1.75×10^{19} s$^{-1}<k_g^0<1.15\times10^{20}$ s^{-1} and 40.5 kJ/mol$<E_a^{k_g}<$47.0 kJ/mol. The error limits for $k_g'^0$ lie between (3.0×10^{18} s^{-1}) and 1.3×10^{22} s^{-1}, while for the corresponding activation energy lies between 45.5 kJ/mol and 78.0 kJ/mol. It would appear for 10B1M7 that the values of k_2 and k_g' are less well determined than the remaining two jump constants. The error limits for $D_\perp^0$ lie between 4.4×10^8 s^{-1} and 1.13×10^9s^{-1}, while 7.9 kJ/mol$<E_a^{D_\perp}<$10.9 kJ/mol. For the spinning motion of 10B1M7, 3.1×10^{16} s$^{-1}<D_\parallel^0<1.0\times10^{17}$ s^{-1} and 47.3 kJ/mol$<E_a^{D_\parallel}<$51.1 kJ/mol. The apparent activation energy for molecular tumblings is smaller than that for the spinning motion as often encountered in NMR studies of liquid crystals [9].

In summary, a global target analysis of spectral densities has been carried out for 10B1M7 in its high temperature Sm-A phase. It is clear that the modified decoupled model appears to give reasonable jump rates for internal dynamics in a flexible chain. The assumptions used in limiting the number of conformations in earlier study of nOCB appear to be valid also for a decyloxy chain of a chiral smectogen. Therefore, we believe that the original decoupled model could fit the chain data of liquid crystals reasonably well by simply forcing the k_3 values to unreasonably high rates. While the jump rate constants of 10B1M7 for the two-bond motion are faster than those for *gauche* pair formations by about two orders of magnitudes, the rates for one-bond jumps and *gauche* migrations are similar and take on intermediate values. All jump rates are found to be faster than the spinning motions of molecules by one or more orders of magnitudes. Although systematic deviations do exist between the calculated and experimental spectral densities, we believe that the modified decoupled model shows great promise for applying to molecules with even longer end chain.

ACKNOWLEDGMENTS

The financial support from the Natural Sciences and Engineering Research Council of Canada and the Italian MURST are gratefully acknowledged. R.Y.D. also thanks the technical support of N. Finlay and R. Shearer.

[1] A.D.L. Chandani, T. Hagiwara, Y. Suzuki, Y. Ouchi, H. Takezoe, and A. Fukuda, Ferroelectrics **85**, 99 (1988).
[2] B. Jin, Z. Ling, Y. Takanishi, K. Ishikawa, H. Takezoe, A. Fukuda, M. Nakimoto, and T. Kitazume, Phys. Rev. E **53**, R4295 (1996).
[3] K.H. Kim, K. Ishikawa, H. Takezoe, and A. Fukuda, Phys. Rev. E **51**, 2166 (1995); **52**, 2120 (1995).
[4] J.W. Goodby, J.S. Patel, and E.J. Chin, J. Mater. Chem. **2**, 197 (1992).
[5] K. Yoshino, Y. Fuwa, K. Nakayama, S. Uto, H. Moritake, and M. Ozaki, Ferroelectrics **197**, 1 (1997).
[6] A. Dahlgren, M. Buivydas, F. Gouda, L. Komitov, M. Matuszczyk, and St. Lagerwall, Liq. Cryst. **25**, 553 (1998).
[7] M. Čepič and B. Žekš, Phys. Rev. Lett. **87**, 085501 (2001).
[8] H. Moritake, K. Nakayama, M. Ozaki, and K. Yoshino, Mol. Cryst. Liq. Cryst. Sci. Technol., Sect. A **263**, 13 (1995).
[9] R. Y. Dong, *Nuclear Magnetic Resonance of Liquid Crystals* (Springer, New York, 1997).
[10] K. Tokumaru, B. Jin, B. Yoshino, Y. Takanishi, K. Ishikawa, H. Takezoe, A. Fukuda, T. Nakai, and S. Miyajima, Jpn. J. Appl. Phys., Part 1 **38**, 147 (1999).
[11] S. Yoshida, B. Jin, Y. Takanishi, K. Tokumaru, K. Ishikawa, H. Takezoe, A. Fukuda, T. Kusumoto, T. Nakai, and S. Miyajima, J. Phys. Soc. Jpn. **68**, 9 (1999).
[12] I. Nishiyama, M. Saito, and A. Yoshizawa, Mol. Cryst. Liq. Cryst. Sci. Technol., Sect. A **263**, 123 (1995).
[13] D. Catalano, M. Cavazza, L. Chiezzi, M. Geppi, and C.A. Veracini, Liq. Cryst. **27**, 621 (2000).
[14] R.Y. Dong, M. Cheng, K. Fodor-Csorba, and C.A. Veracini, Liq. Cryst. **27**, 1039 (2000).
[15] D. Catalano, M. Cifelli, M. Geppi, and C.A. Veracini, J. Phys. Chem. A **105**, 34 (2001).
[16] P. Pincus, Solid State Commun. **7**, 415 (1969).
[17] R.L. Vold, R.R. Vold, and M. Warner, J. Chem. Soc., Faraday Trans. 2 **84**, 997 (1988).
[18] P.L. Nordio and P. Busolin, J. Chem. Phys. **55**, 5485 (1971).
[19] P.L. Nordio, G. Rigatti, and U. Segre, Mol. Phys. **25**, 129 (1973).
[20] J.M. Bernassau, E.P. Black, and D.M. Grant, J. Chem. Phys. **76**, 253 (1982).
[21] R. Tarroni and C. Zannoni, J. Chem. Phys. **95**, 4550 (1991).
[22] R.Y. Dong and G.M. Richards, Chem. Phys. Lett. **171**, 389 (1990); R.Y. Dong, Phys. Rev. A **43**, 4310 (1991).
[23] A. Ferrarini, G.J. Moro, and P.L. Nordio, Liq. Cryst. **8**, 593 (1990).
[24] P. J. Flory, *Statistical Mechanics of Chain Molecules* (Wiley, New York, 1969).
[25] J. Struppe and F. Noack, Liq. Cryst. **20**, 595 (1996).
[26] R.Y. Dong and G.M. Richards, J. Chem. Soc., Faraday Trans. **88**, 1885 (1992).
[27] R.Y. Dong, L. Friesen, and G.M. Richards, Mol. Phys. **81**, 1017 (1994).
[28] R.Y. Dong, Mol. Phys. **88**, 979 (1996).
[29] L. Calucci, M. Geppi, C.A. Veracini, and R.Y. Dong, Chem. Phys. Lett. **296**, 357 (1998).
[30] X. Shen and R.Y. Dong, J. Chem. Phys. **108**, 9177 (1998).
[31] X. Shen, R.Y. Dong, N. Boden, R.J. Bushby, P.S. Martin, and A. Wood, J. Chem. Phys. **108**, 4324 (1998).
[32] R.Y. Dong, Phys. Rev. E **60**, 5631 (1999).
[33] R.Y. Dong, A. Carvalho, P.J. Sebastião, and H.T. Nguyen, Phys. Rev. E **62**, 3679 (2000).
[34] R.Y. Dong and M. Cheng, J. Chem. Phys. **113**, 3466 (2000).
[35] R.Y. Dong, C.R. Morcombe, L. Calucci, M. Geppi, and C.A. Veracini, Phys. Rev. E **61**, 1559 (2000).
[36] R.Y. Dong, Chem. Phys. Lett. **329**, 92 (2000).
[37] R.Y. Dong, J. Chem. Phys. **114**, 5897 (2001).
[38] E. Helfand, J. Chem. Phys. **54**, 4651 (1971).
[39] J. Skolnick and E. Helfand, J. Chem. Phys. **72**, 5489 (1980).
[40] E. Helfand, E.R. Wasserman, and T.A. Weber, Macromolecules **13**, 526 (1980).
[41] J.W. Emsley, G.R. Luckhurst, and C.P. Stockley, Proc. R. Soc. London, Ser. A **381**, 117 (1982).
[42] C. J. R. Counsell, Ph.D. thesis, Southampton, 1983; C.J.R. Counsell, J.W. Emsley, G.R. Luckhurst, and H.S. Sachdev, Mol. Phys. **63**, 33 (1988).
[43] S. Wimperis, J. Magn. Reson. **83**, 590 (1990).
[44] R.Y. Dong and G.M. Richards, J. Chem. Soc., Faraday Trans. 2 **84**, 1053 (1988).
[45] W. H. Press, B. P. Flannery, S. A. Teukolsky, and N. T. Vetterling, *Numerical Recipes* (Cambridge University Press, Cambridge, 1986).